

What can Off-the-Shelves Large Multi-Modal Models do for Dynamic Scene Graph Generation?

Xuanming Cui¹

xuanming.cui@ucf.edu

Jaiminkumar Ashokbhai Bhoi¹

ja882177@ucf.edu

Chionh Wei Peng²

weipeng@dso.org.sg

Adriel Kuek²

kyongjie@dso.org.sg

Ser Nam Lim¹

sernam@ucf.edu

¹University of Central Florida

²DSO National Laboratories

Abstract

Dynamic Scene Graph Generation (DSGG) for videos is a challenging task in computer vision. While existing approaches often focus on sophisticated architectural design and solely use recall during evaluation, we take a closer look at their predicted scene graphs and discover three critical issues with existing DSGG methods: severe precision-recall trade-off, lack of awareness on triplet importance, and inappropriate evaluation protocols. On the other hand, recent advances of Large Multimodal Models (LMMs) have shown great capabilities in video understanding, yet they have not been tested on fine-grained, frame-wise understanding tasks like DSGG. In this work, we conduct the first systematic analysis of Video LMMs for performing DSGG. Without relying on sophisticated architectural design, we show that LMMs with simple decoder-only structure can be turned into State-of-the-Art scene graph generators that effectively overcome the aforementioned issues, while requiring little finetuning (5-10% training data).

1. Introduction

Scene Graph Generation (SGG) aims at generating structured representations for visual contents in the form of scene graph triplets $\langle \text{Subject}, \text{Relation}, \text{Object} \rangle$. Previous works predominantly focus on static SGG under the image modality, by designing complicated architectures to exploit the structural property of SGG with graph-based learning [23, 38, 43, 45, 47], or to better capture the synergy between object detection and relation classification [13, 20, 42], the two major components of existing SGG models. Recently, several works [9, 22, 49] leverage the advances in multi-modal foundational models for image SGG, resulting in the improvements of their performance.

Compared to the advances of SGG in image domain,

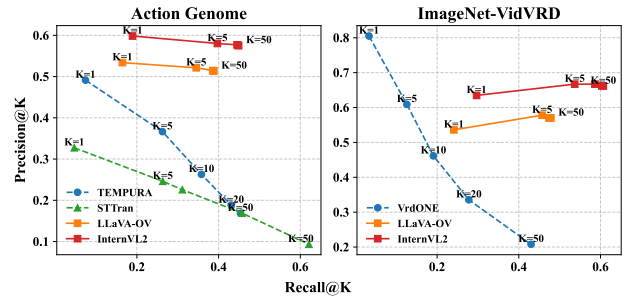


Figure 1. Precision-Recall curve for popular DSGG [5, 15, 30] methods and LLaVA-OneVision [17] on two popular DSGG datasets: Action Genome [14] and ImageNet-VidVRD [34] with top- K predictions where $K \in \{1, 5, 10, 20, 50\}$. We observe severe precision-recall trade-off on existing methods such as STTran [5] on Action Genome, and VrdONE [15] on ImageNet-VidVRD: while existing works mainly report recall with large $K \in \{10, 20, 50\}$, their precisions drop rapidly at the same time, as opposed to LLaVA-OV, whose precision remains stable.

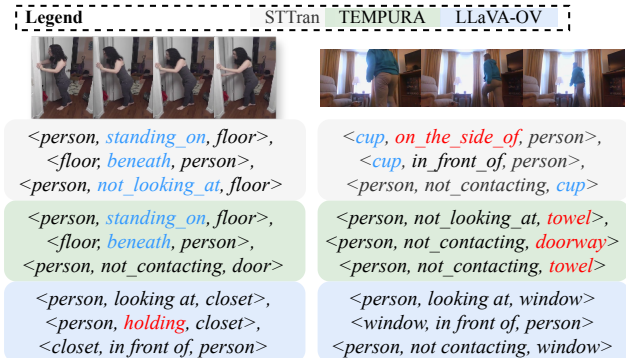


Figure 2. Visualization of top-3 prediction from STTran [5], TEMPURA [30], and LLaVA-OV [17] with two sample video clips from Action Genome [14]. Red denotes incorrect prediction. Light blue denotes entities not being in the ground-truth but semantically correct. While STTran and TEMPURA predicts correct but uninformative triplets such as $\langle \text{person}, \text{standing_on}, \text{floor} \rangle$ (left), LLaVA-OV predicts $\langle \text{person}, \text{looking_at}, \text{closet} \rangle$, the primary activity of the scene.

Dynamic Scene Graph Generation (DSGG) for videos is less explored yet more challenging. Existing works [5,

7, 30, 31, 42, 46] extend image SGG by inserting additional modules to handle temporal relations. Despite the progress in DSGG, a number of limitations exist as follows. (1) Most DSGG modules are trained from scratch, requiring large amount of training data, which is extremely laborious to collect due to frame-wise annotations for both visual relations and localization. (2) DSGG datasets suffer from lack of comprehensiveness [31] and the long-tail distribution problem: annotators tend to use coarse (e.g. $\langle man, on, horse \rangle$) instead of detailed and informative labels (e.g. $\langle man, riding, horse \rangle$), leading to a long-tailed label distribution [30], hindering model performance. Furthermore, we identify three additional issues: (3) **Precision-Recall Trade-Off**: Existing DSGG methods achieve high recall score at the cost of precision (Figure 1). (4) **Lack of awareness on triplet importance**: SGG has been largely formulated as an unordered retrieval task. This formulation overlooks the possibility that the retrieved triplets could be uninformative and redundant (Figure 2). (5) **Inappropriate evaluation methods**: existing DSGG evaluation protocol involves issues such as incomplete metrics (solely reporting recall yet omitting precision), inflated recall (with $Recall@K \gg \#$ of ground-truths), and unrealistic task settings. Please refer to Section 3 for a detailed discussion.

Motivated by the recent success of Large Multimodal Models (LMMs) [6, 26, 54] in video understanding and reasoning [4, 24, 48], we are interested in their performance on fine-grained, frame-wise DSGG task. Although LMMs have shown strong video reasoning capability through several comprehensive benchmarks [8, 41], these benchmarks predominantly focus on holistic video reasoning in the form of short-answer QA, and do not include fine-grained, frame-level scene graph-like annotations. To make up for this, we conducted the *first study* on using LMMs for the DSGG task. While a handful of works have explored utilizing LMMs in SGG [12, 16], they have only considered LMMs for generating synthetic training data. In contrast, we are interested in directly adopting LMMs for SGG because of their strong video understanding and zero-shot capacity [8, 41]. Our study subsequently reveals several advantages of using LMMs for DSGG over existing approaches.

Firstly, given the strong zero-shot visual understanding capacity of pre-trained LMMs, we could alleviate the reliance on intensive human annotation for DSGG, which also mitigates the effect of long-tail distribution problem rooted in manually-labeled DSGG datasets. To evaluate the zero-shot capability of LMMs on DSGG, we utilize a set of meticulously designed prompts and a vocabulary alignment module that maps the novel vocabularies generated by the LMM to the close vocabularies. We find that even though the LMM can suffer from relation hallucination when generating scene graph triplets under the zero-shot setting, likely due to the excessive context length of

the prompt and the generated scene graph, fine-tuning the LMM with as little as 5% of the training data results in a significant performance boost, surpassing state-of-the-art (SOTA) DSGG baseline by a large margin on multiple metrics. This finding means that we can avoid the need to separately train fully supervised models for each specific DSGG tasks and settings, greatly helping to alleviate the tedious annotation process for the DSGG task. Moreover, during fine-tuning, we find that by injecting triplet importance prior into the training data, we can easily enable LMMs to generate scene graph triplets in the order of their importance, as opposed to traditional DSGG methods which tend to assign higher ranks for uninformative triplets.

Secondly, while traditional DSGG models adopt a multi-stage *bottom-up* design, building the scene graph on top of the detector’s regional outputs, LMMs take the video as a whole and performs *top-down*, stage-less video understanding. Compared to traditional DSGGs’ *bottom-up* process, LMMs’ *top-down* approach is more akin to how human perceive and retain visual contents holistically without explicit encoding [29, 36]. Moreover, most existing DSGGs use image-based object detectors as base models. Using these detectors could introduce information loss since these detectors are neither trained to capture object relations nor the holistic semantics of the scene and have no temporal knowledge. We conjecture that, because of these reasons, our experiments show that LMMs are highly robust against the precision-recall trade-off. Further, as LMMs are trained with general video understanding tasks such as video captioning and video QA, they are capable of understanding the primary activities in the scene, and can therefore prioritize semantically important triplets (e.g. $\langle person, looking\ at, closet \rangle$) over uninformative ones (e.g. $\langle floor, beneath, person \rangle$) (Figure 2).

Lastly, we improve the existing DSGG evaluation protocol by measuring both recall and precision across different tasks and K s, adopting a more realistic task setting, and propose to further evaluate DSGG as a ranking task based on the triplet importance.

In summary, our contributions are:

- We identify three critical issues in existing DSGG methods: precision-recall trade-off, the lack of awareness in triplet importance, and the issues with the existing evaluation protocol, and provide a re-evaluation with more comprehensive metrics.
- We perform the first comprehensive analysis on LMMs’ capability on fine-grained, frame-wise video understanding through the task of DSGG. We show that by finetuning with only 5-10% of the training data, we can turn a LMM into an accurate and robust scene graph generator, alleviating various issues in existing DSGG methods including long-tail predicates, precision-recall trade-off, while requiring little human annotations.

- We propose to turn DSGG from an unordered retrieval task into a ranking problem based on triplet importance, and show we can improve baseline LMM scene graph generator to achieve near-perfect ranking performance.

2. Related Work

2.1. Scene Graph Generation

Scene Graph Generation (SGG) provides a structured representation of the visual content. It has been studied extensively for image modality, with approaches focusing on leveraging the graph property of the scene graph via Message Passing [23, 38, 43, 45] and Graph Convolutional Network [25]. Another line of works focuses on handling the long-tailed problem due to coarse labeling [37, 39, 52].

SGG with Multimodal Foundational Models. Recently, several works utilize pre-trained multimodal foundational models for SGG. For instance, VS³ utilizes the pre-trained GLIP [21] for region-word alignment, and [22] treats SGG as an image-to-sequence task by finetuning BLIP [19] for object/predicate prediction as well as localization.

GPT-Assisted SGG. Another line of recent works utilizes Large Language Models (LLMs) to assist SGG. LLM4SGG [16] utilizes ChatGPT to generate scene graph data from image (video) captions to train existing SGG methods for weakly-supervised SGG. Similarly, LASER [12] also leverages ChatGPT to form ground-truth labels, but it converts natural language to formal video specifications and guides the training via a neuro-symbolic alignment score. VLPrompt [53] prompts a LLM to generate likely predicates given subject-object pairs, which are used as auxiliary context for relation prediction.

Instead of using LLMs as an auxiliary module, in this work, we explore the possibility of leveraging LMMs for direct scene graph generation.

2.1.1. Dynamic Scene Graph Generation

Dynamic Scene Graph Generation (DSGG) contains another layer of complexity on top of static SGG due to the additional temporal dimension. Existing methods in DSGG typically resemble similar architectural designs in traditional SGG models but with an extra temporal information aggregation module. For instance, STTran [5] adds an attention module as the temporal decoder on top of the spatial encoder. TRACE [40] uses a 3D CNN for extracting spatial-temporal information and a similar attention-based temporal fusion model. OED [42] follows the similar architectural design but replace Faster-RCNN with DETR [2] as the detection backbone. A few other works [30, 44] focus on the long-tail problem in DSGG, similar to that in static SGG. However, none of the above DSGG methods consider utilizing pre-trained foundational models.

2.2. Large Multimodal Models

Following LLaVA [26]’s success in visual reasoning, a large amount of visual instruction-tuned Large Multimodal Models (LMMs) have been developed [6, 18, 27, 54]. LMMs typically share a similar structure: a visual encoder, a language model backbone, and a lightweight linear projection layer to connect the two. While visual understanding on image modality has been extensively studied, attention has been recently drawn to include video modality [4, 17, 24], by treating videos as multiple images for unified pre-training and instruction tuning [4, 17, 24]. To effectively evaluate LMMs’ understanding and visual reasoning ability, various benchmarks have been developed [8, 10] with questions focusing on different aspects of the visual content. Despite the comprehensiveness in question domain, they are typically in the form of short-answered Q&A format, focusing on the reasoning aspect of the model. However, there is a lack of assessment of LMMs on fine-grained, frame-wise understanding for videos. This work fills this vacancy by evaluating LMMs with DSGG tasks.

3. Limitations in Existing DSGG models

3.1. Inappropriate Evaluation Protocols

Incomplete Metrics: Most SGG works [5, 13, 42, 49] report only recall yet omitting precision. Although this omission is often justified by incomplete ground-truth annotations (where semantically correct predictions may not appear in the ground truth, leading to underestimated precision), it remains problematic. In downstream DSGG tasks such as Visual Question Answering (VQA) or video captioning, false positives are as detrimental as false negatives and significantly impact performance.

Inflated Recall: Most DSGG works report recall@ $K \in \{10, 20, 50\}$ and $K \in \{50, 100\}$ [15, 51]. However, given the average number of ground-truth triplets per frame is often much less than the smallest K (e.g., ~ 7 in Action Genome), reported recall scores are artificially inflated, especially given the absence of precision.

Unrealistic SGCLS Task Setting: Scene Graph Classification (SGCLS) is a main task under DSGG, the purpose of which is to classify the class of subject, object and the relation simultaneously. SGCLS is arguably the most important DSGG task for downstream applications like VQA and video captioning. However, existing works [5, 30] evaluate SGCLS using ground-truth bounding boxes rather than predicted ones. This formulation greatly limits their applicability to manually annotated test datasets.

3.2. Precision-Recall Trade-Off in Existing DSGG

As prior DSGG works mainly focus on the Recall@ K but omit precision, we find their precisions drop substantially

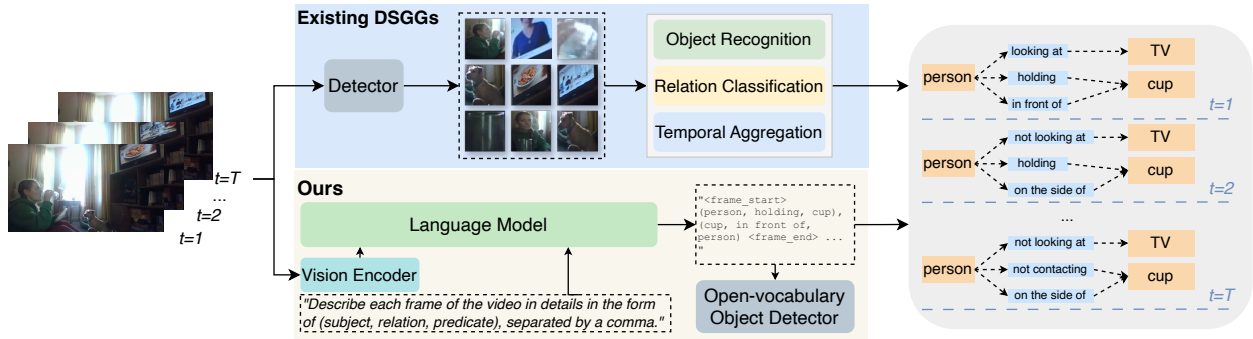


Figure 3. A comparison between existing DSGG pipeline (top) and ours (bottom). Existing DSGG methods typically employ a *bottom-up* approach, where an external detector is used in the first place to extract local features of each detected objects, which are then passed to a series of sub-modules for handling object and relation classification, and temporal aggregation. On the other hand, our approach follows a *top-down* procedure, where the video is first passed to the pre-trained vision encoder and the language model to obtain a holistic understanding. The grounding is done after the scene graph is generated by utilizing a pre-trained open-vocabulary object detector.

when K increases, as can be seen in Figure 1. We conjecture this is due to two reasons. (1) The inflated recall problem discussed above, and (2) due to the bottom-up modular design with each module handling different sub-tasks of DSGG (object detection, objects and relation classification), existing works [5, 42, 50] are effectively factorizing the conditional probability $P(\langle s, p, o \rangle | V)$ into

$$P(\langle s, p, o \rangle | V) = P(D|V)P(s, o|D)P(p|s, o)$$

where $\langle s, p, o \rangle$ denotes the scene graph triplets $\langle \text{subject}, \text{predicate}, \text{object} \rangle$, V denotes the input video and D denotes the detection results. This formulation could easily lead to information loss. Furthermore, the object and relation learning modules from traditional DSGG models [5, 30, 40] are built on top of the regional features extracted by object detectors and trained with classification loss. Although a few recent works [42] specifically target one-stage SGG, they still rely on object detectors which are not trained to capture object relations and the holistic visual content. Moreover, as these object detectors are image-based, they may impose an information bottleneck when used as the primary component with video inputs.

3.3. Lack of awareness on Triplet Importance

In existing literature, DSGG is viewed as an unordered retrieval task. However, in practical scenarios where a scene could potentially involve a large number of scene graph triplets that are uninformative and redundant, it is beneficial to rank important triplets higher. Conversely, due to the long-tail problem, existing methods tend to assign higher probabilities to scene graph triplets that are most prevalent in the training data, which could be less informative. In Figure 2, we show visual comparison of generated top-3 triplets between STTran [5], a popular DSGG model, TEMPURA [30], a DSGG method specifically designed to mitigate long-tailed problem, and LLaVA-OV [17]. We can

see both STTran and TEMPURA promote uninformative triplets (e.g. $\langle \text{person}, \text{standing on}, \text{floor} \rangle$) and redundant triplets $\langle \text{floor}, \text{beneath}, \text{person} \rangle$, whereas LLaVA-OV generates triplets that are relevant to the primary activities in the scene (e.g. $\langle \text{person}, \text{looking at}, \text{closet} \rangle$).

4. Method

4.1. DSGG as Next Token Prediction

Instead of treating scene graphs as graphs with explicit nodes (object) and edges (relations), we regard them as natural language and turn DSGG into a next token prediction task, which LMMs excel at. An overview of the comparison between the DSGG pipeline from existing works and ours is shown in Figure 3. While all traditional DSGG models adopt the *bottom-up* design with the object detector as the base model, followed by specific modules for relation classification, we turn this procedure upside-down by jointly and holistically performing object and relation recognition with an LMM, followed by object grounding using an off-the-shelf object detector. In this way, we can directly model $P(\langle s, p, o \rangle | V)$ without factorization and avoid the potential information loss by building on top of an image-based object detector for video-based DSGG.

4.1.1. Zero-Shot DSGG with Few-shot Prompting

Given the strong Zero-Shot capability of LMMs, we first evaluate their performance on Zero-Shot DSGG. In order to force the model to follow the desired structure, we carefully construct the prompts with few-shot examples of the target scene-graph structures. To refrain from being completely open-vocabulary, we provide a list of objects/predicates and prompt the model to choose from it. Finally, we use a pre-trained language model T5 [33] to map the generated objects/predicates to ground-truth categories. We consider two types of prompt: generating triplets independently for each

frame, and generating each triplet once with the temporal boundary. We found the former to generally perform better. The sample prompt is included in the appendix (Figure 6).

4.1.2. Finetuning LMMs for DSGG

To explore the upper-bound of LMMs’ capacity on DSGG, we further finetune the pre-trained LMMs on DSGG data. We follow the similar prompting strategy under the Zero-Shot setting, and finetune the model using the standard negative log-likelihood loss:

$$\mathcal{L} = - \sum_{t=1}^T \log P(x_t | \mathcal{V}, x_{<t}; \theta_{\text{LMM}})$$

where x_t denotes the t -th token, \mathcal{V} denotes the latent embedding of input video, θ_{LMM} denotes the pretrained LMM. The sample prompt is included in the appendix (Figure 7).

4.1.3. Grounding with Open-Vocabulary Object Detector

Since existing LMMs do not naturally produce dense object localizations in a video, we utilize an open-vocabulary object detector, GroundingDino [28], for grounding generated triplets from the LMM. Given GroundingDino’s capability of Referring Expression Comprehension (grounding objects with attributes), we can turn the generated scene graph triplets into attributes of the subject and object. For instance, given a generated triplet $\langle person, holding, cup \rangle$, we can obtain specifications for subject and object in the form of “*The person holding cup.*” and “*The cup being hold by person.*”. These can then be used as input query to GroundingDino, which is able to identify the object with the given attributes. In case of symmetric triplets, we simply keep the top-2 objects with the correct queries.

4.1.4. Incorporating Triplet’s Importance Prior

We consider two criteria for calculating triplet importance: *informative-ness* – whether the triplet describes the primary activity or visual components in the scene, and *diversity* – how much new information gained from including the new triplet given existing ones. To calculate *informative-ness*, we adopt the CLIP [32] score between the triplet in the form of natural language “*a $\langle s \rangle$ is $\langle p \rangle$ $\langle o \rangle$* ” and the corresponding frame. Since CLIP is trained on image-caption pairs, where captions generally focus on main activities and visual components, the CLIP score provides a reasonable approximation of triplet importance¹. To calculate *diversity*, we take the average pair-wise text similarity between the new and each generated triplets. The resulting triplet importance score is a combination of the two. We refer this as Importance Ranking (IR) in later discussion.

To enable LMM for IR, for Zero-Shot setting, we include few-shot examples with sample triplets appearing in the order of their importance. For finetuning, given the autoregressive nature of LMMs, we can simply rank triplets in

¹We provide a qualitative justification in Sec.2 of the Appendix.

the training data given their importance score to inject such prior to the LMMs.

5. Experiments

5.1. Experimental Setup

5.1.1. Datasets

Following previous works [5, 30, 42] in DSGG, we use the Action Genome (AG) dataset [14]. The AG dataset is a subset of the Charades dataset [35] composed of around 10K videos with scene graph annotations that average 7 scene graph triplets per frame. It contains 35 objects and 25 relation categories. The 25 relations are further divided into three categories: (1) *attention*: whether the person is paying attention to the object, (2) *spatial*: relations between the object and the person and, (3) *contacting*: the actual interaction between the person and the object. Additionally, we also evaluate the model on ImageNet-VidVRD [34] (Vid-VRD), which contains 1,000 videos, with 35 entity categories, 132 predicate categories, and 11 triplets per frame.

5.1.2. Evaluation Metrics

Tasks. We consider two standard tasks from DSGG: (1) Scene Graph Classification (SGCLS): given ground-truth bounding boxes of subjects/objects, predict the subject/object and relation, and (2) (SGDet²): detect subjects/objects and predict relations, where the detection is successful if the Intersection over Union (IoU) is at least 0.5. We adopt the *No Constraints* setting, where for each predicted Subject-Object pair we consider multiple predicted predicates, as it best reflects LMMs’ video understanding capacity and is a more realistic task setting. To provide a comprehensive evaluation, we report both Recall@ K and Precision@ K for Action Genome and Vid-VRD, where $K \in \{1, 10, 20, 50, 100\}$ denotes the top- K triplets per frame. To consider the top- K triplets for LMM generated scene graphs, we simply take the first K generated triplets, based on the observation that perplexity increases proportional to generation length [1].

From SGCLS to SGCLS*. On top of standard SGCLS, we make a modification: instead of taking ground-truth bounding box, we use the predicted bounding box. This is because (1) LMMs do not receive ground-truth bounding boxes as input, so this setting ensures a fair comparison, and (2) this makes the task more realistic since we cannot assume manually-annotated bounding boxes to be available at test time. We denote this variation as SGCLS*. To calculate SGCLS*, we simply adopt the SGDet calculation function by changing IoU from 0.5 (default threshold in SGDet) to 0, thereby removing the grounding criteria.

²Note while SGDet in [5, 30, 42] calculates IoU separately for each frame, the equivalent task ReIDet [15] aggregates IoU over consecutive frames, and the triplet is correct if the aggregated IoU is greater than 0.5.

Dataset	Model	% Data	Recall					Precision				
			@1	@10	@20	@50	@100	@1	@10	@20	@50	@100
Action Genome	STTran	-	0.047	0.311	0.457	0.621	0.663	0.327	0.226	0.169	0.093	0.050
	TEMPURA	-	0.074	0.378	0.485	0.597	0.632	0.491	0.273	0.180	0.090	0.048
	OED	-	0.074	0.443	0.559	0.668	0.735	0.541	0.352	0.228	0.110	0.060
	Video-LLaVA	Zero-Shot	0.013	0.017	0.017	0.018	0.0178	0.047	0.030	0.029	0.029	0.029
	LLaVA-OV		0.040	0.066	0.067	0.067	0.067	0.152	0.126	0.126	0.126	0.126
	InternVL2		0.049	0.094	0.100	0.111	0.112	0.161	0.124	0.121	0.121	0.121
	Video-LLaVA	5%	0.045	0.153	0.158	0.158	0.158	0.178	0.152	0.150	0.150	0.150
	LLaVA-OV		0.123	0.260	0.261	0.261	0.261	0.406	0.389	0.389	0.389	0.389
	InternVL2		0.140	0.274	0.295	0.295	0.295	0.482	0.455	0.452	0.452	0.452
	Video-LLaVA	100%	0.109	0.289	0.293	0.293	0.293	0.374	0.339	0.336	0.336	0.336
	LLaVA-OV		0.165	0.386	0.388	0.388	0.388	0.534	0.515	0.514	0.514	0.514
	InternVL2		0.189	0.397	0.445	0.448	0.448	0.598	0.580	0.576	0.575	0.575
ImageNet VidVRD	VrdONE	-	0.033	0.191	0.278	0.430	0.569	0.805	0.462	0.336	0.208	0.138
	Video-LLaVA	Zero-Shot	0.010	0.023	0.023	0.024	0.024	0.027	0.025	0.024	0.024	0.024
	LLaVA-OV		0.041	0.096	0.097	0.097	0.097	0.113	0.089	0.088	0.089	0.089
	InternVL2		0.018	0.027	0.027	0.027	0.027	0.033	0.026	0.026	0.026	0.026
	Video-LLaVA	10%	0.004	0.005	0.005	0.005	0.005	0.011	0.010	0.010	0.010	0.010
	LLaVA-OV		0.237	0.451	0.453	0.453	0.453	0.493	0.506	0.505	0.505	0.505
	InternVL2		0.242	0.476	0.480	0.482	0.482	0.535	0.552	0.551	0.551	0.551
	Video-LLaVA	100%	0.216	0.437	0.447	0.449	0.449	0.463	0.496	0.494	0.492	0.492
	LLaVA-OV		0.276	0.501	0.503	0.503	0.503	0.532	0.565	0.565	0.565	0.565
	InternVL2		0.295	0.582	0.596	0.602	0.602	0.625	0.661	0.655	0.654	0.654

Table 1. Evaluation results on SGCLS* under Action Genome [14] and ImageNet-VidVRD [34]. We re-evaluate the previous methods under SGCLS* for both recall and precision. Best results are bold in **Black**. **Dark green** indicates that the 5%/10%-finetuned LMM beats the existing SOTA baselines.

DSGG as a ranking task. While existing DSGG evaluation focuses on unordered retrieval, it would also be informative to evaluate how well DSGG models are able to rank the retrievals based on their relevancy (*i.e.* importance). We adopt Normalized Discounted Cumulative Gain (nDCG):

$$DCG_p = \sum_{i=1}^p \frac{2^{rel_i} - 1}{\log_2(i + 1)}, nDCG_p = \frac{DCG_p}{IDCG_p}$$

where p refers to the rank position, rel_i is the importance score for triplet i , and $IDCG_p$ refers to the ideal DCG_p calculated from the ground-truth³.

5.1.3. Implementation Details

We conduct our experiments mainly using LLaVA-OneVision [17] (LLaVA-OV) and InternVL2 [3]. We use GroundingDino [28] as the open-vocabulary object detector due to its strong Referring Expression Comprehension (REC) ability. To map unseen objects/relations from the LMMs’ generation to ground-truth vocabulary, we use T5 encoder [33] to calculate cosine similarity between the predicted and the ground-truth vocabulary for the matching. For finetuning, we use the standard LoRA [11] fine-tuning procedure, and train for 1 epoch under all experiments.

Baselines We compare our method with prior SOTA works on DSGG including STTran [5], TEMPURA [30],

OED [42] for AG, and VrdOne [15]. for VidVRD, by re-evaluating the baselines under SGCLS* task as discussed in Section 5.1.2. We also re-evaluate SGDNet to obtain a comprehensive evaluation for both precision and recall.

5.2. Results

SGCLS* and SGDNet. Tables 1 and 2 present results for SGCLS* and SGDNet across baseline methods and our approach. In the Zero-Shot setting, LMMs exhibit low accuracy in SGCLS*, primarily due to vocabulary misalignment—where the model predicts objects or predicates that are not in the ground-truth vocabulary even though they are often semantically correct—and severe predicate hallucination (further discussed in Section 6). However, finetuning on just 5%-10% of the training data for one epoch significantly improves performance. For instance, on VidVRD, LLaVA-OV achieves an R@10 of 0.451, compared to VrdONE’s 0.191. With full-dataset fine-tuning, LMMs achieve state-of-the-art performance across multiple K s. On VidVRD, InternVL2 attains an R@10 of 0.582, outperforming VrdONE by 40%. Table 2 summarizes SGDNet results: on Action Genome, InternVL2 surpasses OED with an R@10 of 0.362 vs. 0.340 and a P@1 of 0.553 vs. 0.436.

DSGG with Importance Ranking. In Table 3 we show quantitative performance of the SGCLS* task before and after applying Importance Ranking (IR) on the Action Genome dataset. We can observe a noticeable increase in

³The calculation of $nDCG_p$ is detailed in Sec.4 in the appendix.

Dataset	Model	% Data	Recall					Precision				
			@1	@10	@20	@50	@100	@1	@10	@20	@50	@100
Action Genome	STTran	100%	0.037	0.248	0.332	0.356	0.360	0.263	0.176	0.131	0.071	0.038
	TEMPURA		0.057	0.290	0.369	0.451	0.474	0.380	0.210	0.137	0.068	0.036
	OED		0.059	0.340	0.424	0.500	0.549	0.436	0.272	0.174	0.083	0.045
	LLaVA-OV	5%	0.095	0.202	0.202	0.202	0.202	0.387	0.383	0.383	0.383	0.383
	InternVL2		0.102	0.218	0.224	0.224	0.224	0.451	0.416	0.412	0.412	0.412
	LLaVA-OV	100%	0.143	0.355	0.355	0.355	0.355	0.504	0.493	0.493	0.493	0.493
InternVL2	0.159		0.362	0.382	0.386	0.386	0.553	0.529	0.525	0.525	0.525	
ImageNet-VidVRD	VrdONE	100%	0.022	0.101	0.136	0.182	0.216	0.530	0.245	0.164	0.088	0.052
	LLaVA-OV	10%	0.203	0.432	0.437	0.437	0.437	0.466	0.468	0.468	0.468	0.468
	InternVL2		0.209	0.445	0.448	0.448	0.448	0.482	0.497	0.491	0.491	0.491
	LLaVA-OV	100%	0.246	0.491	0.491	0.491	0.491	0.508	0.542	0.535	0.535	0.535
InternVL2		0.253	0.511	0.514	0.514	0.514	0.531	0.547	0.542	0.542	0.542	

Table 2. Evaluation results on SGDet task under Action Genome and ImageNet-VidVRD. We rerun previous methods’ SGDet metric to obtain precision and additional K s. Best results are bold in **black**. **Dark green** indicates that the 5%/10%-finetuned LMM beats the SOTA baselines.

Model	Mode	nDCG ₅	R@10	P@10
TEMPURA	-	0.49	0.38	0.27
OED	-	0.51	0.44	0.35
LLaVA-OV	Zero-Shot	0.67	0.067	0.13
	+IR	0.79 (+0.11)	0.065	0.13
	Fine-tuned	0.63	0.39	0.52
	+IR	1.00 (+0.37)	0.39	0.53 (+0.02)
	InternVL	Zero-Shot	0.59	0.094
+IR	0.69 (+0.17)	0.097	0.13	
Fine-tuned	0.76	0.40	0.58	
+IR	1.00 (+0.24)	0.40	0.59 (+0.012)	

Table 3. Quantitative results for nDCG₅ under SGCLS* on Action Genome before and after Importance Ranking (IR.), for Zero-Shot and Finetuned settings.

nDCG under the Zero-Shot setting, indicating the LMM is capable of understanding the importance of triplets through few-shot prompting. Under finetuning, both models’s nDCGs increase significantly and reach 1, meaning their rankings are as good as the ground-truth’s. On the other hand, baseline methods’ nDCG is noticeably lower than baseline LMMs, as they tend to promote prevalent triplets which are often less semantically important. Meanwhile, as a byproduct of IR, we observe a slight increase in precision (*e.g.* 0.02 for LLaVA-OV). We conjecture the improvement is because the ground-truth annotation after IR aligns better with how LMMs are trained to describe a scene.

LMMs are balanced scene graph generator. In Table 1 for SGCLS* and Table 2 for SGDet, we can observe that the LMMs produced much more balanced performance between precision and recall when compared to prior works, which all suffer from severe precision-recall trade-off. For instance, OED achieves SOTA results on Action Genome for R@50, yet only scores 0.093 under P@50. On the other hand, under VidVRD, while VrdONE achieves the SOTA P@1 of 0.805, it drops to 0.462 with P@10, with a R@10

%Data	Triplet		Subject		Predicate		Object	
	P.	R.	P.	R.	P.	R.	P.	R.
Z.S.	0.09	0.10	0.90	0.79	0.12	0.12	0.89	0.80
5%	0.51	0.45	0.92	0.90	0.58	0.54	0.92	0.90
10%	0.55	0.48	0.94	0.93	0.62	0.55	0.94	0.93
100%	0.57	0.50	0.95	0.95	0.64	0.57	0.95	0.94

Table 4. The breakdown of Precision and Recall for individual subjects, objects and predicates for LLaVA-OV on VidVRD. **Z.S.** denotes the Zero-Shot setting. **P.** and **R.** denote precision and recall. Here we do not specify K because we are considering all the generation from the LMM.

of 0.191. Meanwhile, the precision of LLaVA-OV finetuned with 5% data increases from 0.493 to 0.506 when K increases from 1 to 10, with a R@10 score of 0.451. This suggests LLaVA-OV has a much more balanced precision-recall performance, implying its stronger holistic video understanding capacity compared to prior DSGG models.

6. Ablations

Performance on Individual Entity/Predicate In Table 4 we show results on precision/recall on individual subject, object and predicates. We can observe that under all settings, the precision and recall for both subjects and objects are high, with precision and recall at around 0.9, while the predicate’s accuracy is substantially lower. For example, under Zero-Shot setting, the precision is only 0.12 for predicates. This shows LLaVA-OV is mainly restrained by the predicate accuracy, which is reasonable as predicates are more complex and open-ended.

Predicate Hallucination and Effect of Finetuning Figure 4 shows qualitative results before (grey) and after (green) finetuning. Interestingly, although the generated video descriptions are accurate and detailed, the corresponding scene graphs immediately following these de-

Prompt: "Describe the video in details. Based on the description, generate scene graph triplets in the form of (subject, predicate, object) for each frame, based on the description."



Figure 4. LLaVA-OV’s generation before and after finetuning with 5% training data. Wrong predicates are highlighted in red.

	Subject ↓	Predicate ↓	Object ↓
Zero-Shot	0.96	0.87	0.97
Fine-tuned	0.99	0.51	0.93

Table 5. Perplexity for Subject/Predicate/Object on VidVRD with LLaVA-OV before and after finetuning.

Descriptions often exhibit significant hallucinations, particularly in the predicate predictions. For example, in the second example, while the description accurately captures a man riding a motorcycle and performing a sharp turn, the associated scene graph includes the correct objects but incorrect predicates, such as *feed* and *walk left*. After finetuning with 5% of the training data for one epoch, these hallucinations are significantly reduced and the model yields accurate predicates. In Table 5 we additionally show perplexity before and after finetuning. We can see the perplexity reduces significantly for predicates, from 0.87 to 0.51, while stay mostly the same for Subject and Object, indicating the predicates are the major source of hallucinations.

We hypothesize that these hallucinations come from two factors: (1) the excessive context length due to video data, long in-context examples, and lengthy generated scene graphs, which considerably deviate from training data such as video captioning and video QA, and (2) identifying relations is a more complex task than identifying objects, and current LMMs may still fall behind on it under the long-context, fine-grained scenario in DSGG.

LMM on Long-tailed Predicates Since long-tail problem is a central challenge in traditional SGG, here we analyze how LMM performs on rare classes. In Table 6 we show that LLaVA-OV significantly outperforms TEMPURA [30], a model specifically designed to handle long-tailed distribution, on mean class precision and mean recall. In Figure 5, we further compare the Recall/Precision per predicate category between LLaVA-OV and TEMPURA [30]. We can see that without specific unbiased training, LLaVA-OV achieves similar or better performance on Recall@5 and Recall@10, especially on the rare predicates (to the right of each plot). On the other hand, we can observe LLaVA-OV outperforms TEMPURA on Precision with a larger margin, especially for the long-tailed

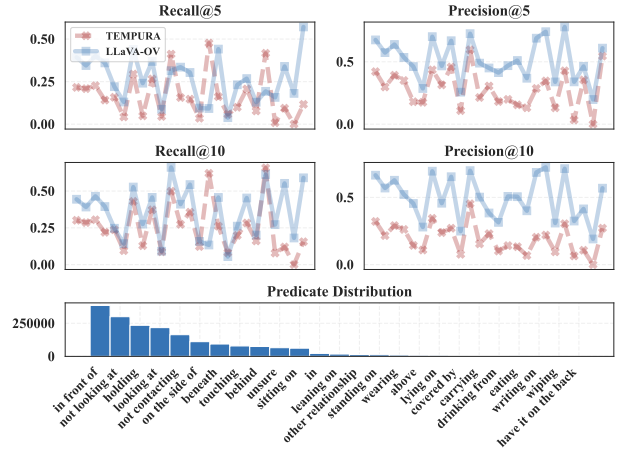


Figure 5. Per predicate class Recall/Precision performance between LLaVA-OV (orange) and TEMPURA (blue) with $K \in \{5, 10\}$ on Action Genome, under SGCLS*. LLaVA-OV is finetuned with 5% training data. The predicate categories are sorted from highest to lowest based on the number of occurrence.

Model	mR				mP			
	@1	@5	@10	@20	@1	@5	@10	@20
TEMPURA	0.03	0.15	0.24	0.33	0.31	0.27	0.18	0.11
LLaVA-OV	0.07	0.31	0.33	0.33	0.58	0.54	0.53	0.53

Table 6. Comparison of predicate class-wise mean recall (mR) and precision (mP) on SGCLS* under Action Genome.

categories, suggesting LMM is unbiased towards these rare predicates. While this is expected as we only finetune the LMM for limited amount of steps, it still also signifies the importance of utilizing foundational models for SGG.

7. Conclusion

In this work, we address the problem of Dynamic Scene Graph Generation (DSGG) using Large Multimodal Models (LMMs). Our study reveals that with minimal finetuning, LMMs achieve state-of-the-art performance, surpassing prior approaches by a considerable margin. Furthermore, our results demonstrate that leveraging LMMs for DSGG effectively mitigates issues such as long-tailed prediction and the precision-recall trade-off.

What can Off-the-Shelves Large Multi-Modal Models do for Dynamic Scene Graph Generation?

Supplementary Material

8. Training details

We finetune LoRAs for LLaVA-OV and Video-LLaVA using a single H100 GPU, while two H100 GPUs are used for training LoRAs on InternVL2. The LoRA rank is set to 256 with an alpha value of 512 across all experiments, each trained for a single epoch. The learning rates are configured as follows: 2×10^{-5} for Video-LLaVA, 1×10^{-5} for LLaVA-OV, and 4×10^{-5} for InternVL2. Batch sizes are set to 1 for LLaVA-OV, 16 for Video-LLaVA, and 4 for InternVL2. We conduct experiments with 5% (1000 samples) and 100% of the training data on Action Genome, 10% (1000 samples) and 100% on VidVRD.

9. Qualitative justification for Importance Ranking with CLIP score

We utilize CLIP [32] score between each triplet and the corresponding frame to measure *informative-ness*. In Figure 6 we show examples of triplets ranked by their CLIP [32] score with the corresponding frames. We can see triplets depicting primary activities (e.g. $\langle person, holding, bottle \rangle$) or major visual components (e.g. $\langle laptop, on, table \rangle$) receive higher scores, compared to less important triplets (e.g. $\langle floor, beneath, person \rangle$).

10. Details for Triplet Importance Calculation

We calculate Triplet Importance (TI) based on a combination of triplet *informative-ness* T_I and triplet *diversity* T_D . Given an image I and i -th corresponding triplet T_i , $TI = \lambda T_I + (1 - \lambda) T_D$ with:

$$T_I = \cos(\text{Enc}_i(I), \text{Enc}_t(T_j))$$
$$T_D = \begin{cases} 1, & \text{if } i = 1 \\ 1 - \frac{1}{i-1} \sum_{k=1}^{i-1} \cos(\text{Enc}_t(T_k), \text{Enc}_t(T_i)), & \text{otherwise} \end{cases}$$

where $\cos(\cdot, \cdot)$ denotes the cosine similarity function, Enc_i and Enc_t denotes CLIP’s image and text encoder. We experimentally set $\lambda = 0.75$ to give a higher weight for T_I , as T_D ’s scale of change is often larger than T_I ’s, which outweighs the former.

11. Details for nDCG Calculation

We use normalized Discounted Cumulative Gain (nDCG) as the ranking metric. Recall the definition of nDCG is:

$$DCG_p = \sum_{i=1}^p \frac{2^{rel_i} - 1}{\log_2(i + 1)}, nDCG_p = \frac{DCG_p}{IDCG_p}$$

where p refers to the rank position, rel_i is the importance score for triplet i , and $IDCG_p$ refers to the ideal DCG_p . To obtain $IDCG$, we rank the ground-truth triplets by their importance TI , and calculate their DCG_p . Due to the incompleteness of human-annotated ground-truth scene graph data, sometime the LMM could generate triplets with higher TI than the ground-truth. Therefore, we cap $nDCG$ to be max 1, i.e. $nDCG_p = \min(\frac{DCG_p}{IDCG_p}, 1)$.

12. Additional Qualitative Results for Importance Ranking

In Table 7 we show the three most predicted predicates for the Top-1 triplet predicted by TEMPURA, LLaVA-OV, and LLaVA-OV trained with triplet Importance Ranking (IR). While TEMPURA’s three most often predicted predicates are less informative (e.g. *not looking at*), LLaVA-OV’s is slightly better, but still contains un-informative predicates such as *unsure*. On the other hand, LLaVA-OV with IR’s most often predicted predicates are more specific and activity-related (e.g. *holding*).

In Figure 7 we show the average CLIP score for the Top-5 triplets predicted by each models. We can observe LLaVA-OV trained with IR has a clear decreasing trend, suggesting it is able to capture the informative-ness prior added to the training data.

13. Additional qualitative results

Comparison between Zero-Shot and Finetuned LMM Generation. Figure 8 shows the qualitative comparison between the output of zero-shot and fine-tuned LMM on Dynamic Scene Graph Generation (DSGG). As we can observe, fine-tuning significantly increases the number of generated triplets while also improves the accuracy and reduces hallucinations. For example, in the right column, the Zero-shot generation incorrectly identifies the notebook as laptop and that the person is looking at the laptop, and predicts limited triplets. In contrary, the finetuned generation produces more triplets that are both diverse and accurate.



Figure 6. Examples of CLIP [32] scores between triplets and frames from Action Genome [14]. Triplets are sorted in descending order based on CLIP score.

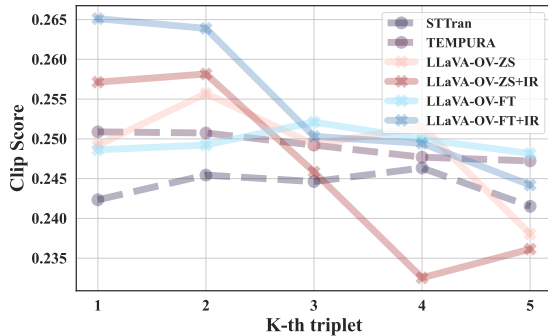


Figure 7. Top-5 triplets’ CLIP score generated by STTran [5], TEMPURA [30], LLaVA-OV under Zero-Shot (ZS) and fine-tuned (FT) settings, with or without triplet Importance Ranking (IR), under Action Genome [14] dataset.

Comparison between LMM and Previous methods.

Figure 9 and Figure 10 compare scene graph generated from STTran [5], TEMPURA [30], LLaVA-OV, and LLaVA-OV with Importance Ranking (IR). We can observe STTran and TEMPURA are able to generate more triplets but also exhibit a higher rate of false positives, including the generation of context-based triplets—instances where triplets are produced even when the corresponding objects are absent from the scene. In contrast, LLaVA-OV-based results are noticeably more accurate. We can observe that as the number of predictions increases, STTran and TEMPURA tend to generate more false positives, leading to a decline in precision at higher values of K . In contrast, LLaVA-OV effectively aligns triplet generation with the scene context, maintaining higher precision. Meanwhile, we can also observe from both Figure 9 and Figure 10 that previous methods like STTran and TEMPURA tends predict prevalent objects and relations such as "floor" and "not looking at" as the highest confidence entities and relations. However, in the given examples, these

TEMPURA	LLaVA-OV	LLaVA-OV(+ IR)
<i>not looking at</i>	<i>looking at</i>	<i>holding</i>
<i>in front of</i>	<i>not looking at</i>	<i>touching</i>
<i>not contacting</i>	<i>unsure</i>	<i>looking at</i>

Table 7. Top-3 frequent relations predicted by TEMPURA, LLaVA-OV and LLaVA-OV(+IR.) at the Top-1 triplet.

entities and relations are either not visible in the scene, or are not important to the primary activity. On the other hand, LLaVA-OV with Importance Ranking (IR) is able to generate the most relevant triplets first. For instance, for the right most sample of Figure 10, where the person is sitting on a chair while reading a book, while STTran predicts $\langle \text{floor}, \text{beneath}, \text{person} \rangle$, LLaVA-OV is able to predict $\langle \text{person}, \text{looking at}, \text{cabinet} \rangle$, which is more relevant to the person’s action. Meanwhile, by training with IR, the results also involve less redundant triplets at a rank position. Take the same example for instance, while STTran predicts redundant triplets: $\langle \text{chair}, \text{beneath}, \text{person} \rangle$, $\langle \text{person}, \text{sitting on}, \text{chair} \rangle$, $\langle \text{chair}, \text{behind}, \text{person} \rangle$, LLaVA + IR is able to predict distinct distinct triplets up to a rank position.

14. Prompts

Figure 11 illustrates the ZS prompt used to generate quadruplets $\langle \text{subject}, \text{action}, \text{spatial}, \text{object} \rangle$ for the VidVRD dataset. In VidVRD, predicates are designed as combinations of action and spatial predicates. By separating these into two distinct components, the prompt includes fewer predicates, resulting in improved performance compared to using triplets where action and spatial predicates are merged into a single predicate. Figure 12 presents the fine-tuning prompt used for training the Video-LLaVA-Vicuna, LLaVA-OV and InternVL2 models. Instead of using quadruplets—specific to the VidVRD dataset de-

		
Ground-truth	<p><person, not looking at, sofa/couch>, <sofa/couch, behind, person>, <person, holding, dish> <sofa/couch, beneath, person>, <person, sitting on, sofa/couch>, <person, leaning on, sofa/couch>, <person, unsure, food>, <food, in front of, person>, <person, holding, food>, <person, not looking at, dish>, <dish, in front of, person></p>	<p><person, looking at, book>, <book, in front of, person>, <person, touching, book>, <person, holding, book>, <person, looking at, paper/notebook>, <paper/notebook, in front of, person>, <person, holding, paper/notebook>, <person, writing on, paper/notebook>, <person, not looking at, bed>, <bed, beneath, person>, <bed, above, person>, <bed, in front of, person>, <bed, on the side of, person>, <person, sitting on, bed></p>
Zero-Shot LLaVA-OV	<p><person, not looking at, sofa>, <laptop, in front of, person>, <sofa, behind, person>, <person, eating, laptop></p>	<p><person, not looking at, table>, <laptop, in front of, person>, <table, on the side of, person>, <person, looking at, laptop></p>
Finetuned LLaVA-OV	<p><person, not looking at, sofa/couch>, <sofa/couch, beneath, person>, <sofa/couch, behind, person>, <person, sitting on, sofa/couch>, <person, leaning on, sofa/couch>, <person, not looking at, food>, <food, in front of, person>, <person, holding, food>, <person, not looking at, dish>, <dish, in front of, person>, <person, holding, dish>, <person, not looking at, table>, <table, in front of, person>, <person, not contacting, table></p>	<p><person, looking at, book>, <book, in front of, person>, <person, touching, book>, <person, looking at, paper/notebook>, <paper/notebook, in front of, person>, <person, writing on, paper/notebook>, <person, not looking at, floor>, <floor, beneath, person>, <person, sitting on, floor></p>
Finetuned LLaVA-OV + IR	<p><person, holding, food>, <person, sitting on, sofa/couch>, <table, in front of, person>, <sofa/couch, behind, person>, <person, leaning on, sofa/couch>, <dish, in front of, person>, <person, not looking at, dish>, <person, not looking at, sofa/couch>, <sofa/couch, beneath, person>, <person, not looking at, food>, <person, not looking at, dish></p>	<p><person, writing on, paper/notebook>, <person, sitting on, floor>, <person, looking at, book>, <book, in front of, person>, <person, touching, book>, <person, looking at, paper/notebook>, <paper/notebook, in front of, person>, <floor, beneath, person></p>

Figure 8. Comparison between LLaVA-OV’s Zero-Shot, fine-tuned, and fine-tuned with Importance Ranking generation on Action Genome [14]. The trend shows an increase in the number of triplets generated, with a notable improvement in the alignment of triplets to the ground truth. Predicates/entities highlighted in red indicate incorrect results. Predicates/entities highlighted in light blue (i.e. laptop, in front of, a person) are not part of the ground truth but are factually correct and visible in the scene. Triplets are displayed (top-down) in the order of their model predictions (sorted by probability for STTran and TEMPURA, or by their order of generation for LLaVA-OV).

sign—the triplet format is employed for fine-tuning, as it is universally applicable across all datasets. The fine-tuning prompt is designed to separate the triplets of each frame by a unique token `#frameid` as well as `#sgend` unique token which is used to indicate stop for generating more tokens, it

also helps in avoiding repetitive token generation.

References

- [1] Sourya Basu, Govardana Sachitanandam Ramachandran, Nitish Shirish Keskar, and Lav R. Varshney. Mirostat: A neu-



Ground-truth

<person, unsure, laptop>, <laptop, in front of, person>
 <person, not contacting, laptop>, <person, not looking at, table>
 <table, in front of, person>, <person, touching, table>

<person, looking at, groceries>, <groceries, in front of, person>,
 <person, holding, groceries>, <person, looking at, food>,
 <food, in front of, person>, <person, holding, food>,
 <person, looking at, shelf>, <shelf, in front of, person>,
 <person, not contacting, shelf>, <person, looking at, bag>,
 <bag, in front of, person>, <person, holding, bag>

TEMPURA

<person, not looking at, light>, <person, not contacting, light>
 <person, not contacting, light>, <light, above, person>
 <person, not looking at, light>, <light, above, person>
 <person, not looking at, book>, <book, in front of, person>
 <light, on the side of, person>, <person, not contacting, book>

<door, on the side of, person>, <person, not contacting, door>,
 <door, in front of, person>, <person, not contacting, doorway>,
 <doorway, in front of, person>, <doorway, on the side of, person>,
 <person, not contacting, door>, <door, in front of, person>,
 <person, touching, door>, <door, on the side of, person>,
 <person, not contacting, pillow>, <pillow, on the side of, person>

STTran

<person, not contacting, light>, <light, in front of, person>
 <light, on the side of, person>, <person, not contacting, light>
 <light, in front of, person>. <light, on the side of, person>
 <person, not contacting, table>, <table, in front of, person>
 <person, touching, table>, <person, not contacting, television>

<clothes, on the side of, person>, <person, wearing, clothes>,
 <person, not contacting, clothes>, <person, holding, clothes>,
 <person, not contacting, shelf>, <shelf, in front of, person>,
 <shelf, on the side of, person>, <person, wearing, clothes>,
 <clothes, on the side of, person>, <person, not contacting, clothes>,
 <vacuum, on the side of, person>, <person, holding, vacuum>

Finetuned
LLaVA-OV

<person, unsure, book>, <book, on the side of, person>
 <person, touching, book>, <person, unsure, laptop>
 <laptop, in front of, person>, <person, not contacting, laptop>

<person, looking at, food>, <food, in front of, person>,
 <person, holding, food>, <person, not looking at, closet/cabinet>,
 <closet/cabinet, in front of, person>, <person, holding, groceries>,
 <person, not contacting, cabinet>, <person, looking at, groceries>,
 <groceries, in front of, person>, <person, not looking at, doorway>,
 <doorway, on the side of, person>, <person, not contacting, doorway>

Finetuned
LLaVA-OV + IR

<laptop, in front of, person>, <book, on the side of, person>
 <person, touching, table>, <person, unsure, laptop>
 <person, unsure, book>, <person, touching, book>,
 <person, not contacting, laptop>

<person, looking at, food>, <person, holding, food>,
 <food, in front of, person>, <closet/cabinet, in front of, person>,
 <person, holding, groceries>, <person, looking at, groceries>,
 <groceries, in front of, person>
 <person, not looking at, closet/cabinet>,
 <person, not contacting, cabinet>

Figure 9. Qualitative comparison between Tempura, STTran, and LLaVA-OV. Predictions/objects highlighted in red represent false predictions. Predicates/objects that are contextually relevant (i.e., the objects and relationships visible in the video) but not in the ground-truth annotations are highlighted in light blue. Triplets are displayed (top-down) in the order of their model predictions (sorted by probability for STTran and TEMPURA, or by their order of generation for LLaVA-OV).

ral text decoding algorithm that directly controls perplexity, 2021. 5

- [2] Nicolas Carion, Francisco Massa, Gabriel Synnaeve, Nicolas Usunier, Alexander Kirillov, and Sergey Zagoruyko. End-to-end object detection with transformers, 2020. 3
- [3] Zhe Chen, Weiyun Wang, Hao Tian, Shenglong Ye, Zhangwei Gao, Erfei Cui, Wenwen Tong, Kongzhi Hu, Jiapeng Luo, Zheng Ma, et al. How far are we to gpt-4v? closing the gap to commercial multimodal models with open-source

suites. *arXiv preprint arXiv:2404.16821*, 2024. 6

- [4] Zhe Chen, Jiannan Wu, Wenhai Wang, Weijie Su, Guo Chen, Sen Xing, Muyan Zhong, Qinglong Zhang, Xizhou Zhu, Lewei Lu, Bin Li, Ping Luo, Tong Lu, Yu Qiao, and Jifeng Dai. Internvl: Scaling up vision foundation models and aligning for generic visual-linguistic tasks, 2024. 2, 3
- [5] Yuren Cong, Wentong Liao, Hanno Ackermann, Michael Ying Yang, and Bodo Rosenhahn. Spatial-temporal transformer for dynamic scene graph generation.

			
Ground-truth	<p><person, not looking at, phone>, <phone, above, person>, <phone, on the side of, person>, <person, holding, phone></p>	<p><person, looking at, food>, <food, in front of, person>, <person, holding, food>, <person, looking at, sandwich>, <sandwich, in front of, person>, <person, holding, sandwich>, <person, not looking at, bed>, <bed, in front of, person>, <bed, on the side of, person>, <person, other relationship, bed></p>	<p><person, looking at, book>, <book, in front of, person> <person, holding, book>, <person, touching, book>. <person, looking at, paper/notebook>. <paper/notebook, in front of, person> <person, holding, paper/notebook>. <person, not looking at, chair> <chair, beneath, person>. <chair, behind, person></p>
STTran	<p><phone, on the side of, person>, <person, holding, phone>, <person, not looking at, phone>, <phone, on the side of, person>, <person, holding, phone>, <person, not looking at, phone>, <person, not contacting, doorway>, <doorway, in, person>, <doorway, on the side of, person>, <person, not contacting, doorway></p>	<p><floor, beneath, person>, <person, standing on, floor>, <person, other relationship, floor>, <person, not contacting, picture>, <picture, in front of, person>, <person, sitting on, floor>, <person, unsure, picture>, <picture, on the side of, person>, <person, unsure, floor>, <person, not contacting, book></p>	<p><floor, beneath, person>, <chair, beneath, person> <person, sitting on, chair>, <chair, behind, person> <person, leaning on, chair>, <person, not looking at, chair> <person, sitting on, floor>, <person, other relationship, floor> <person, standing on, floor>, <shoe, beneath, person></p>
LLaVA-OV	<p><person, not looking at, phone>, <phone, on the side of, person>, <person, holding, phone></p>	<p><person, not looking at, sandwich>, <sandwich, in front of, person>, <person, holding, sandwich>, <person, eating, sandwich></p>	<p><person, looking at, book>, <book, in front of, person> <person, holding, book>, <person, not looking at, chair> <chair, beneath, person>, <chair, behind, person> <person, sitting on, chair>, <person, leaning on, chair></p>
LLaVA-OV + IR	<p><person, holding, phone>, <person, in, doorway>, <person, on the side of, door>, <phone, on the side of, person>, <person, not looking at, door>, <person, not contacting, door></p>	<p><person, holding, food>, <bed, on the side of, person>, <person, eating, sandwich>, <person, holding, sandwich>, <sandwich, in front of, person>, <person, not contacting with, bed></p>	<p><person, looking at, book>, <person, sitting on, chair>, <person, in, doorway>, <book, in front of, person> <person, holding, book>, <chair, beneath, person>, <person, not looking at, chair></p>

Figure 10. Qualitative examples of generations from LLaVA-OV and STTran. Predictions/objects highlighted in red represent false predictions. Predicates/objects that are contextually relevant (i.e., the objects and relationships visible in the video) but not in the ground-truth annotations are highlighted in light blue. Triplets are displayed (top-down) in the order of their model predictions (sorted by probability for STTran and TEMPURA, or by their order of generation for LLaVA-OV).

CoRR, abs/2107.12309, 2021. 1, 3, 4, 5, 6, 2

[6] Wenliang Dai, Junnan Li, Dongxu Li, Anthony Meng Huat Tiong, Junqi Zhao, Weisheng Wang, Boyang Li, Pascale

Fung, and Steven Hoi. Instructblip: Towards general-purpose vision-language models with instruction tuning, 2023. 2, 3

- [7] Shengyu Feng, Subarna Tripathi, Hesham Mostafa, Marcel Nassar, and Somdeb Majumdar. Exploiting long-term dependencies for generating dynamic scene graphs, 2022. 2
- [8] Chaoyou Fu, Yuhan Dai, Yondong Luo, Lei Li, Shuhuai Ren, Renrui Zhang, Zihan Wang, Chenyu Zhou, Yunhang Shen, Mengdan Zhang, et al. Video-mme: The first-ever comprehensive evaluation benchmark of multi-modal llms in video analysis. *arXiv preprint arXiv:2405.21075*, 2024. 2, 3
- [9] Tao He, Lianli Gao, Jingkuan Song, and Yuan-Fang Li. Towards open-vocabulary scene graph generation with prompt-based finetuning, 2022. 1
- [10] Dan Hendrycks, Collin Burns, Steven Basart, Andy Zou, Mantas Mazeika, Dawn Song, and Jacob Steinhardt. Measuring massive multitask language understanding, 2021. 3
- [11] Edward J. Hu, Yelong Shen, Phillip Wallis, Zeyuan Allen-Zhu, Yanzhi Li, Shean Wang, Lu Wang, and Weizhu Chen. Lora: Low-rank adaptation of large language models, 2021. 6
- [12] Jiani Huang, Ziyang Li, Mayur Naik, and Ser-Nam Lim. Laser: A neuro-symbolic framework for learning spatial-temporal scene graphs with weak supervision, 2024. 2, 3
- [13] Jinbae Im, JeongYeon Nam, Nokyoung Park, Hyungmin Lee, and Seunghyun Park. Egtr: Extracting graph from transformer for scene graph generation, 2024. 1, 3
- [14] Wei Ji, Ranjay Krishna, Li Fei-Fei, and Juan Carlos Niebles. Action genome: Actions as composition of spatio-temporal scene graphs. In *Proceedings of the IEEE/CVF Conference on Computer Vision and Pattern Recognition*, pages 10236–10247, 2020. 1, 5, 6, 2, 3
- [15] Xinjie Jiang, Chenxi Zheng, Xuemiao Xu, Bangzhen Liu, Weiyang Zheng, Huaidong Zhang, and Shengfeng He. Vr-done: One-stage video visual relation detection. In *Proceedings of the 32nd ACM International Conference on Multimedia*, page 1437–1446. ACM, 2024. 1, 3, 5, 6
- [16] Kibum Kim, Kanghoon Yoon, Jaehyeong Jeon, Yeonjun In, Jinyoung Moon, Donghyun Kim, and Chanyoung Park. Llm4sgg: Large language models for weakly supervised scene graph generation, 2024. 2, 3
- [17] Bo Li, Yuanhan Zhang, Dong Guo, Renrui Zhang, Feng Li, Hao Zhang, Kaichen Zhang, Peiyuan Zhang, Yanwei Li, Ziwei Liu, and Chunyuan Li. Llava-onevision: Easy visual task transfer, 2024. 1, 3, 4, 6
- [18] Feng Li, Renrui Zhang, Hao Zhang, Yuanhan Zhang, Bo Li, Wei Li, Zejun Ma, and Chunyuan Li. Llava-next-interleave: Tackling multi-image, video, and 3d in large multimodal models, 2024. 3
- [19] Junnan Li, Dongxu Li, Caiming Xiong, and Steven Hoi. Blip: Bootstrapping language-image pre-training for unified vision-language understanding and generation, 2022. 3
- [20] Jiankai Li, Yunhong Wang, Xiefan Guo, Ruijie Yang, and Weixin Li. Leveraging predicate and triplet learning for scene graph generation, 2024. 1
- [21] Liunian Harold Li, Pengchuan Zhang, Haotian Zhang, Jianwei Yang, Chunyuan Li, Yiwu Zhong, Lijuan Wang, Lu Yuan, Lei Zhang, Jenq-Neng Hwang, Kai-Wei Chang, and Jianfeng Gao. Grounded language-image pre-training, 2022. 3
- [22] Rongjie Li, Songyang Zhang, Dahua Lin, Kai Chen, and Xuming He. From pixels to graphs: Open-vocabulary scene graph generation with vision-language models, 2024. 1, 3
- [23] Yikang Li, Wanli Ouyang, Bolei Zhou, and Xiaogang Wang. Vip-cnn: Visual phrase guided convolutional neural network. In *Proceedings of the IEEE Conference on Computer Vision and Pattern Recognition*, pages 1347–1356, 2017. 1, 3
- [24] Bin Lin, Yang Ye, Bin Zhu, Jiayi Cui, Munan Ning, Peng Jin, and Li Yuan. Video-llava: Learning united visual representation by alignment before projection, 2024. 2, 3
- [25] Xin Lin, Changxing Ding, Jinquan Zeng, and Dacheng Tao. Gps-net: Graph property sensing network for scene graph generation, 2020. 3
- [26] Haotian Liu, Chunyuan Li, Qingyang Wu, and Yong Jae Lee. Visual instruction tuning, 2023. 2, 3
- [27] Haotian Liu, Chunyuan Li, Yuheng Li, and Yong Jae Lee. Improved baselines with visual instruction tuning, 2024. 3
- [28] Shilong Liu, Zhaoyang Zeng, Tianhe Ren, Feng Li, Hao Zhang, Jie Yang, Qing Jiang, Chunyuan Li, Jianwei Yang, Hang Su, Jun Zhu, and Lei Zhang. Grounding dino: Marrying dino with grounded pre-training for open-set object detection, 2024. 5, 6
- [29] Neil W. Mulligan and Miri Besken. 220 Implicit Memory. In *The Oxford Handbook of Cognitive Psychology*. Oxford University Press, 2013. 2
- [30] Sayak Nag, Kyle Min, Subarna Tripathi, and Amit K Roy-Chowdhury. Unbiased scene graph generation in videos. In *Proceedings of the IEEE/CVF Conference on Computer Vision and Pattern Recognition*, pages 22803–22813, 2023. 1, 2, 3, 4, 5, 6, 8
- [31] Trong-Thuan Nguyen, Pha Nguyen, and Khoa Luu. Hig: Hierarchical interlacement graph approach to scene graph generation in video understanding, 2024. 2
- [32] Alec Radford, Jong Wook Kim, Chris Hallacy, Aditya Ramesh, Gabriel Goh, Sandhini Agarwal, Girish Sastry, Amanda Askell, Pamela Mishkin, Jack Clark, Gretchen Krueger, and Ilya Sutskever. Learning transferable visual models from natural language supervision, 2021. 5, 1, 2
- [33] Colin Raffel, Noam Shazeer, Adam Roberts, Katherine Lee, Sharan Narang, Michael Matena, Yanqi Zhou, Wei Li, and Peter J. Liu. Exploring the limits of transfer learning with a unified text-to-text transformer, 2023. 4, 6
- [34] Xindi Shang, Tongwei Ren, Jingfan Guo, Hanwang Zhang, and Tat-Seng Chua. Video visual relation detection. In *Proceedings of the 25th ACM International Conference on Multimedia*, page 1300–1308, New York, NY, USA, 2017. Association for Computing Machinery. 1, 5, 6
- [35] Gunnar A. Sigurdsson, Gül Varol, Xiaolong Wang, Ali Farhadi, Ivan Laptev, and Abhinav Gupta. Hollywood in homes: Crowdsourcing data collection for activity understanding, 2016. 5
- [36] Sruthi Sridhar, Abdulrahman Khamaj, and Manish Asthana. Cognitive neuroscience perspective on memory: overview and summary. *Frontiers in Human Neuroscience*, 17, 2023. 2
- [37] Shuzhou Sun, Shuaifeng Zhi, Qing Liao, Janne Heikkilä, and Li Liu. Unbiased scene graph generation via two-stage causal modeling, 2023. 3

- [38] Kaihua Tang, Hanwang Zhang, Baoyuan Wu, Wei Luo, and Ting Liu. Neural motifs: Scene graph parsing with global context. In *Proceedings of the IEEE Conference on Computer Vision and Pattern Recognition*, pages 5831–5840, 2018. 1, 3
- [39] Kaihua Tang, Yulei Niu, Jianqiang Huang, Jiaxin Shi, and Hanwang Zhang. Unbiased scene graph generation from biased training, 2020. 3
- [40] Yao Teng, Limin Wang, Zhifeng Li, and Gangshan Wu. Target adaptive context aggregation for video scene graph generation, 2021. 3, 4
- [41] Andong Wang*, Bo Wu*, Sunli Chen, Zhenfang Chen, Hao-tian Guan, Wei-Ning Lee, Erran Li Li, Joshua B Tenenbaum, and Chuang Gan. Sok-bench: A situated video reasoning benchmark with aligned open-world knowledge. In *The IEEE/CVF Conference on Computer Vision and Pattern Recognition (CVPR)*, 2024. 2
- [42] Guan Wang, Zhimin Li, Qingchao Chen, and Yang Liu. Oed: Towards one-stage end-to-end dynamic scene graph generation, 2024. 1, 2, 3, 4, 5, 6
- [43] Danfei Xu, Yuke Zhu, Christopher B. Choy, and Li Fei-Fei. Scene graph generation by iterative message passing. *arXiv (Cornell University)*, 2017. 1, 3
- [44] Li Xu, Haoxuan Qu, Jason Kuen, Jiuxiang Gu, and Jun Liu. Meta spatio-temporal debiasing for video scene graph generation, 2022. 3
- [45] Jianwei Yang, Jiasen Lu, Stefan Lee, Dhruv Batra, and Devi Parikh. Graph r-cnn for scene graph generation. In *Proceedings of the European conference on computer vision (ECCV)*, pages 670–685, 2018. 1, 3
- [46] Jingkang Yang, Wenxuan Peng, Xiangtai Li, Zujin Guo, Liangyu Chen, Bo Li, Zheng Ma, Kaiyang Zhou, Wayne Zhang, Chen Change Loy, and Ziwei Liu. Panoptic video scene graph generation, 2023. 2
- [47] Alireza Zareian and Shih-Fu Chang Karaman. Scene graphs and beyond: Visual understanding with structured representations. In *Proceedings of the IEEE International Conference on Computer Vision Workshops*, pages 5858–5867, 2019. 1
- [48] Hang Zhang, Xin Li, and Lidong Bing. Video-llama: An instruction-tuned audio-visual language model for video understanding, 2023. 2
- [49] Yong Zhang, Yingwei Pan, Ting Yao, Rui Huang, Tao Mei, and Chang-Wen Chen. Learning to generate language-supervised and open-vocabulary scene graph using pre-trained visual-semantic space. In *2023 IEEE/CVF Conference on Computer Vision and Pattern Recognition (CVPR)*, pages 2915–2924, 2023. 1, 3
- [50] Yong Zhang, Yingwei Pan, Ting Yao, Rui Huang, Tao Mei, and Chang-Wen Chen. End-to-end video scene graph generation with temporal propagation transformer. *IEEE Transactions on Multimedia*, 26:1613–1625, 2024. 4
- [51] Sipeng Zheng, Shizhe Chen, and Qin Jin. Vrdformer: End-to-end video visual relation detection with transformers. In *2022 IEEE/CVF Conference on Computer Vision and Pattern Recognition (CVPR)*, pages 18814–18824, 2022. 3
- [52] Zijian Zhou, Miaoqing Shi, and Holger Caesar. Hilo: Exploiting high low frequency relations for unbiased panoptic scene graph generation, 2023. 3
- [53] Zijian Zhou, Miaoqing Shi, and Holger Caesar. Vlprompt: Vision-language prompting for panoptic scene graph generation, 2024. 3
- [54] Deyao Zhu, Jun Chen, Xiaoqian Shen, Xiang Li, and Mohamed Elhoseiny. Minigt-4: Enhancing vision-language understanding with advanced large language models, 2023. 2, 3

{USER}: Your task is to create meaningful quadruplets which describe the provided video. Quadruplets consist of subject, action relation, spatial relation, and object.

The objects are:

bus,motorcycle,sheep,frisbee,antelope,turtle,lizard,airplane,train,horse,giant_panda,bird,hamster,elephant,ball,watercraft,red_panda,rabbit,bear,whale,domestic_cat,lion,bicycle,monkey,squirrel,sofa,snake,car,tiger,fox,skateboard,zebra,dog,cattle,person.

The relationship consists of two entities: 1. action and 2. spatial.

The action relations are: bite,chase,creep,drive,fall,off,faster,feed,fight,fly,fly with, follow,hold,jump,jump with,kick,larger,lie,lie inside,lie with,move,move with,play,pull,ride, run,run with,sit,sit inside,stand,stand inside,stand with,stop,stop with,swim,swim,with,taller,touch,walk,walk,with,watch.

The spatial relations are:toward,past,above,left,beneath,right,behind,away,front,next to.

Step-1: List all unique objects present in the provided video using the objects list provided and assign random IDs to them for tracking.

Step-2: Describe all possible relationships between objects obtained in Step-1 using the relationship lists provided.

Ensure every spatial and action relation between each pair is captured in a detailed manner.

For each object pair, provide a list of multiple spatial relations (e.g., front, left, right, etc.).

Step-3: Provide quadruplets in the format <object-id, action, spatial, object-id> using Step-1 and Step-2, ensuring all possible spatial and action relations are described for each pair of objects.

Example output:

```
#sg_start
{
  "objects": ["person-1", "person-2", "dog-3"],
  "quadruplets": [
    ["person-1", "sit", "front", "person-2"],
    ["person-1", "sit", "left", "person-2"],
    ["person-1", "sit", "beneath", "person-2"],
    ["person-1", "sit", "behind", "person-2"],
    ["person-1", "sit", "next to", "dog-3"],
    ["dog-3", "sit", "front", "person-2"],
    ["person-2", "sit", "above", "dog-3"]
  ]
}
#sg_end
"""
```

Figure 11. Example of zero-shot quadruplet generation (subject, action predicate, spatial predicate, object) prompt on the VidVRD dataset. LLaVA-OV demonstrates strong object recognition capabilities; therefore, objects are listed first and assigned unique IDs. This approach helps the model track objects effectively and minimizes the creation of repetitive triplets for the same objects. Triplets are displayed (top-down) in the order of their model predictions (sorted by probability for STTran and TEMPURA, or by their order of generation for LLaVA-OV).

{USER}: You are given a list of predefined subjects, objects, and predicates. Your task is to predict scene graph triplets in the format **[Subject-id:Object-id:Predicate]** based on the given scene in the video. Use only the provided lists for subject, objects, and predicates.

Subjects: turtle,dog,lion,whale,lizard,monkey,bird,bus,ball,bear,train,airplane,hamster,cattle,fox,elephant,horse,skateboard,watercraft,rabbit,domestic_cat,sheep,giant_panda,red_panda,car,motorcycle,squirrel,frisbee,snake,bicycle,person,zebra,sofa,antelope,tiger.

Objects: giant_panda,frisbee,lion,bird,squirrel,monkey,sofa,rabbit,whale,domestic_cat,bear,bus,red_panda,sheep,tiger,person,fox,elephant,antelope,train,skateboard,motorcycle,airplane,bicycle,cattle,snake,zebra,watercraft,dog,lizard,turtle,horse,hamster,car,ball.

Predicates: fly behind,move with,sit above,creep right,jump above,stand beneath,move next to,taller,sit next to,past,walk behind,stand above,touch,run toward,chase,stand inside,sit right,stand left,jump behind,lie front,walk right,run with,run behind,fall off,jump left,walk next to,fly past,swim left,stop beneath,right,sit front,lie right,walk toward,stop left,walk away,move beneath,next to,faster,behind,move past,jump front,lie above,feed,jump past,fight,pull,follow,stop with,front,fly right

{GPT}:

```
#frameid[squirrel-0:domestic_cat-1:sit front];
[domestic_cat-1:squirrel-0:walk behind];
[domestic_cat-1:squirrel-0:walk toward];
#sgend
```

Figure 12. Fine-tuning prompt and response used for training the Action Genome and VidVRD datasets for triplet generation. The #frameid token serves as a unique frame separator, while the #sgend token acts as a stop indicator, signaling the completion of scene graph generation. These tokens help prevent repeated or hallucinated outputs during training.